Title: Selective Deletion of Sodium Salt Taste during Development Leads to Expanded Terminal Fields of Gustatory Nerves in the Adult Mouse Nucleus of the Solitary Tract.

Authors: Sun C, Hummler E, Hill DL

Journal: The Journal of neuroscience : the official journal of the Society for Neuroscience

Year: 2017 Jan 18

Volume: 37

Issue: 3

Pages: 660-672

DOI: 10.1523/JNEUROSCI.2913-16.2017

Selective Deletion of Sodium Salt Taste During Development Leads to Expanded Terminal Fields of Gustatory Nerves in the Adult Mouse Nucleus of the Solitary Tract.

Chengsan Sun[1], Edith Hummler[2], and David L. Hill[1]
[1]Department of Psychology
PO Box 400400, University of Virginia,
Charlottesville, VA 22904-4400
and
[2]Pharmacology and Toxicology Department
Faculty of Biology and Medicine
University of Lausanne, CH-1005
Lausanne, Switzerland.

Abbreviated Title: Taste Activity Dependent Terminal Field Plasticity

Corresponding Author: Dr. David L. Hill
Department of Psychology
PO Box 400400
University of Virginia
Charlottesville, VA 22904
dh2t@virginia.edu
telephone: (434) 982-4728
fax: (434) 982-4785

Number of pages: 34 pages

Number of figures: 7

Number of tables: 0

Number of words: Abstract -- 249

Introduction -- 584

Discussion -- 1467

Conflict of Interest: The authors declare no competing financial interests.

Acknowledgements: This work was supported by National Institutes of Health Grant DC00407 (to DLH) and by the Swiss National Science Foundation Grant 31003A 163347/1 (to EH).

ABSTRACT

Neuronal activity plays a key role in the development of sensory circuits in the mammalian brain. In the gustatory system, experimental manipulations now exist, through genetic manipulations of specific taste transduction processes, to examine how specific taste qualities (i.e., basic tastes) impact the functional and structural development of gustatory circuits. Here, we used a mouse knockout model in which the transduction component used to discriminate sodium salts from other taste stimuli was deleted in taste bud cells throughout development. We used this model to test the hypothesis that the lack of activity elicited by sodium salt taste impacts the terminal field organization of nerves that carry taste information from taste buds to the nucleus of the solitary tract (NST) in the medulla. The glossopharyngeal, chorda tympani, and greater superficial petrosal nerves were labeled to examine their terminal fields in adult control mice and in adult mice in which the alpha subunit of the epithelial sodium channel was conditionally deleted in taste buds (αENaC knockout). The terminal fields of all three nerves in the NST were up to 2.7X greater in αENaC knockout mice compared to the respective field volumes in control mice. The shapes of the fields were similar between the two groups; however, the density and spread of labels were greater in αENaC knockout mice. Overall, our results show that disruption of the afferent taste signal to sodium salts has widespread effects on the development of the terminal fields of nerves that carry taste messages to the brain.

SIGNIFICANCE STATEMENT

Neural activity plays a major role in the development of sensory circuits in the mammalian brain. To date, there has been no direct test if taste-elicited neural activity has a role in shaping central gustatory circuits. However, recently developed genetic tools now allow an assessment of how specific taste stimuli, in this case sodium salt taste, play a role in maturation of the terminal

fields in the mouse brainstem. We found that specific deletion of sodium salt taste during development produced terminal fields in adults that were dramatically larger than in control mice, demonstrating for the first time that sodium salt taste elicited activity is necessary for the normal maturation of gustatory inputs into the brain.

INTRODUCTION

The role of experience on the development of central sensory circuits has been of keen interest in neuroscience since the early work by Hubel and Wiesel (Hubel and Wiesel, 1962). While most studies on this topic center on cortical development, work focused on lower neural level circuits show some, but usually lesser amounts of, dependence on neural activity. For example, in the retinogeniculate pathway, terminal fields of retinal ganglion cells in the dorsal lateral geniculate nucleus dLGN are shaped by intrinsic waves of activity in the retina before the eyes open (Katz and Shatz, 1996; Hooks and Chen, 2006). These circuits are ultimately refined through competitive, activity-dependent mechanisms at about the time, and extending after, the eyes open (Chen and Regehr, 2000; Hooks and Chen, 2006; Ziburkus and Guido, 2006). Thus, both spontaneous and visually-evoked stimuli help orchestrate the organization of visual inputs into the dLGN.

By comparison, little is known about the subcortical development of the gustatory system -- circuits intimately involved in driving feeding and motivated behaviors (Spector and Travers, 2005; Spector and Glendinning, 2009). We do know, however, that some of the anatomical hallmarks characteristic of other developing sensory neural structures occur in the developing gustatory system (Mistretta and Hill, 2003; Mangold and Hill, 2008). Cranial nerves that innervate taste buds in the rodent tongue and palate initially have relatively large and overlapping terminal fields in the nucleus of the solitary tract (NST) in the medulla (Mangold

and Hill, 2008). These profuse projections then decrease dramatically in size at around the time of weaning (Sollars et al., 2006; Mangold and Hill, 2008), which is about the age when taste-elicited activity (especially to NaCl) increases over two fold in magnitude. While there is converging evidence that taste-elicited neural activity plays a role in this postnatal refinement of terminal fields (Hill and Bour, 1985; Vogt and Hill, 1993; Mangold and Hill, 2008; Corson and Hill, 2011), no direct test of this hypothesis has been available.

Recently, however, the ability to selectively alter taste experience to a specific stimulus has been provided by Chandrashekar et al. (2010). They showed that the transduction channel for sodium taste could be deleted from mouse taste bud cells throughout development. Moreover, they found that adult mice lacking the functional sodium salt taste transducer throughout life had a selective suppression of salt taste responses from the chorda tympani nerve, which innervates taste buds on the anterior tongue. They also demonstrated that mice lacking the functional transducer for salt taste lacked the appropriate behavioral responses driven by NaCl (Chandrashekar et al., 2010). Because taste nerve responses to NaCl begin in rodents at about postnatal day 11 (Hill and Bour, 1985) and then changes the most to adulthood (Hill and Almli, 1980; Yamada, 1980; Ferrell et al., 1981), this knockout mouse is an ideal experimental model to ask questions related to the role of taste-elicited activity on the development and plasticity of central gustatory circuits. We show here that, indeed, lack of sodium taste throughout development has profound effects on how nerves that carry taste information project to their central targets. Unexpectedly, the terminal fields of all nerves, even of one that does not carry sodium salt taste information, are permanently affected by this genetic deletion. Our results suggest that there is a lack of maturation of the terminal fields due to the loss of sodium salt taste activity. This is the first clear

demonstration that alteration of a single taste modality is critical for the normal development of taste-related circuits.

MATERIALS AND METHODS

Animals. All experiments were approved by the University of Virginia Animal Care and Use Committee and followed guidelines set forth by the National Institutes of Health and the Society for Neurosciences. To examine the role of lack of sodium salt taste on the development of terminal field organization in the rostral nucleus of the solitary tract (NST), we used mice described in detail by Chandrasekhar et al., 2010. Briefly, the alpha subunit of the epithelial sodium channel (αENaC) was conditionally deleted in taste bud cells by crossing mice that drove the expression of Cre-recombinase under the cytokeratin 19 (CreK19) promotor (Chandrashekar et al., 2010) with mice that were homozygous mutant for the floxed *Scnn1a* (αENaC) gene (*Scnn1a*$^{flox/flox}$) (Hummler et al., 2002). The CreK19 mice were generously supplied by Dr. Charles Zuker, and Dr. Edith Hummler supplied the *Scnn1a*$^{flox/flox}$ mice. Therefore, our experimental animals had the genotype K19-Cre *Scnn1a*$^{flox/flox}$ (αENaC knockout; n=6). The control group consisted of mice that were littermates to experimental animals, but did not have the CreK19 promoter (*Scnn1a*$^{flox/flox}$; n=4) or lacked K19-Cre and *Scnn1a*$^{flox/flox}$ (n=3). We subsequently found no differences in any of our measures for these two groups of control mice; thus, we pooled data from all 7 mice (Controls). All animals were between 60 – 120 days old at the time of the experiments, and both male and female mice were used.

Tissue Collection. To establish that the mice used here had *Scnn1a* removed in the tongue, we used real time quantitative PCR (QPCR) procedures similar to that of Huang and Krimm (2010) and Sun et al. (2015).

Briefly, the anterior 2/3 of fresh tongues from αENaC knockout (n = 4) and control (n = 4) mice were collected and cut at the midline, rinsed with cold PBS, and then incubated in sterile dispase I-solution (BD Biosciences; Franklin Lakes, NJ) for 60 min at 37°C. Epithelial sheets of the tongue were then peeled from the underlying mesenchyme and immediately processed for RNA extraction.

RNA Extraction and QPCR. Total RNA was extracted using RNeasy mini kit (Qiagen; Chatsworth, CA). Traces of DNA were eliminated in samples by treatment with DNase I. Total RNA was analyzed as described in detail in Sun et al. (2015). Reverse transcription was performed using 200 U Superscript III Reverse Transcriptase (ThermoFisher Scientific, Waltham MA) and 50 ng random hexamers in 25 ml reaction volumes following the manufacturer's protocol with the same amount (50 ng) of total RNA. QPCR was performed by 7500 Fast Real-Time PCR System (ThermoFisher Scientific, Waltham, MA) using the Taq-Man Universal PCR Kit. Assays of αENaC and GAPDH (Cat. # 4331182, Mm00803386_m1 and Mm99999915_g1, respectively) were purchased from ThermoFisher Scientific (Waltham, MA). PCR efficiencies were determined by performing PCR with serial (10-fold) dilutions of cDNA in parallel. All samples were run in parallel with the housekeeping gene, mouse glyceraldehyde 3-phosphate dehydrogenase (GAPDH), to normalize cDNA loading. Each assay was carried out in triplicate. PCR was performed for 40 cycles at 95°C for 15 secs and at 60°C for 1 min.

QPCR Analyses. For QPCR, the comparative $2^{-\Delta\Delta CT}$ method was used to determine the relative *Scnn1a* gene expression levels (Huang and Krimm, 2010; Sun et al., 2015).

Fluorescent Anterograde Nerve Labeling. Procedures used to label three nerves with fluorescent tracers were the same as that described previously in mouse (Sun et al., 2015). Briefly, the chorda tympani (CT), greater superficial (GSP), and the glossopharyngeal (IX) nerves were

labeled with anterograde tracers to determine the volume and densities of label among gustatory afferent terminal fields in the NST. The CT carries taste information from taste buds in fungiform papillae on the anterior tongue and the anterior foliate papillae on the posterior tongue to the NST. The GSP carries taste information from taste buds on the soft palate, the geschmacksstreifen, and the nasoincisor duct in the palate to the NST. The IX carries taste information from taste buds in the circumvallate papilla and the posterior foliate papillae, both on the posterior tongue, to the NST (see Sun et al., 2015 for diagram of innervation patterns).

All animals were between 3 and 4 months old at the time of nerve labeling, which are ages beyond the age when mature-like terminal field organization occurs (Mangold and Hill, 2008). Mice were sedated with a 0.32 mg/kg injection of Domitor® (medetomidine hydrochloride: Pfizer Animal Health, Exton, PA; I.M.) and anesthetized with 40 mg/kg Ketaset® (ketamine hydrochloride: Fort Dodge Animal Health, Fort Dodge, IA; I.M.). A water-circulating heating pad was used to maintain body temperature. Using the same surgical approach as detailed in Sun et al., (2015), crystals of 3kD tetramethylrhodamine dextran amine were applied to the proximal cut end of the GSP, crystals of 3kD biotinylated dextran amine were applied to the proximal cut end of the CT, and crystals of 3kD cascade blue dextran amine were applied to the proximal cut end of the IX. A small amount of Kwik-Sil (World Precision Instruments, Inc.; Sarasota, FL) was then placed over the cut end of the nerves to prevent crystals from diffusing from the site of the intended label. All dextran amine conjugates were purchased from Thermofisher Scientific (Waltham, MA). Animals were then injected with 5 mg/ml Antisedan® (atipamezole hydrochloride: Pfizer Animal Health, Exton, PA; I.M) to promote reversal of anesthesia. Following 48-hour survival, animals were deeply anesthetized with urethane and transcardially perfused with Krebs-Henseleit buffer (pH 7.3), followed by 4% paraformaldehyde (pH 7.2).

Tissue preparation. Brains were removed, postfixed, and the medulla was blocked and sectioned horizontally on a vibratome at 50µm (Sun et al., 2015). We chose to section tissue in the horizontal plane because it allows visualization of the entire rostral-caudal and medial lateral extent of the terminal fields in the NST with the smallest number of sections (~10 sections/mouse). It is also the plane in which the axons branch from the solitary tract and primarily project medially in rodents (Davis, 1988; Whitehead, 1988; Lasiter et al., 1989).

Sections were then incubated for 1 hour in PBS containing 0.2% Triton with 1:400 streptavidin Alexa Fluor 647 (Jackson ImmunoResearch Labs, Inc., West Grove, PA) and 1:400 rabbit anti-Cascade Blue (ThermoFisher, Waltham, MA) at room temperature. Streptavidin Alexa Fluor 647 was used to visualize the biotinylated dextran amine-labeled CT positive terminals. Rabbit anti-Cascade Blue was used as a primary antibody to detect Cascade Blue labeled IX terminal fields and was followed with a 1 hr. reaction with 1:400 donkey anti-rabbit Alexa Fluor 488 (Jackson ImmunoResearch Labs, Inc.; West Grove, PA). This secondary antibody was used to visualize IX nerve terminals. Visualization of tetramethylrhodamine, which labeled GSP terminal fields, did not require further processing. Sections were mounted on slides and coverslipped with Vectashield Hardset Mounting Medium (Vector Laboratories, Burlingame, CA).

Confocal Microscopy and Analyses of Terminal Fields.

Imaging. Terminal fields were imaged using a Nikon 80i microscope fitted with a Nikon C2 scanning system (Nikon Instruments, Inc., Melville, NY) and a 10X objective (Nikon, CFIPlanApo; NA=0.45). The nerve labels were matched for the wavelengths of the three lasers in the system (argon laser - 488 nm, 10 mW, IX; DPSS laser - 561 nm, 10mW, GSP; Modulated Diode laser - 638 nm, 20 mW, CT). Sequential optical sections were captured every 3µm for

each 50μm section. Images were obtained with settings adjusted so that pixel intensities were near (but not at) saturation. A transmitted light image at 4X (Nikon PlanFluor; NA=0.13) and at 10X was captured for every physical section containing the labeled terminal field. This permitted an accurate registration of dorsal to ventral brainstem sections among animals within and between groups using common brainstem landmarks (4X), and identification of NST borders (10X).

Analyses of Total Terminal Field Volume. Methods used to analyze terminal field volumes and densities were described previously in detail (Sun et al., 2015). Briefly, quantification of terminal field volume was achieved through the use of custom ImageJ-based software (Sun et al., 2015). Each image stack was rotated so that all images were in the same x-y plane for analyses. The IsoData thresholder algorithm (Ridler and Calvard, 1978) was then applied to yield a binary image stack of the pixels above threshold, followed by particle analysis to quantify the pixel area above threshold for each channel. Volumes from each physical section were summed to yield the total terminal field volume for each mouse. The resultant volume represents an unbiased experimenter measure of the amount of label. Additionally, the volume of colocalization between the terminal fields of two nerves (CT with GSP, GSP with IX, CT with IX) and among all three nerves (CT, GSP, and IX) was determined in a similar manner as described for each single label. Axons (e.g., the solitary tract) were included along with the terminal field for all animals in our analyses because of the difficulty in accurately deleting axons and tracts from each optical section. Accordingly, the absolute volumes that we show here include the composite terminal field and axons. There was no obvious reorganization of nerve tracts among groups; therefore, we make the assumption that including the solitary tract in our measurements had a similar quantitative effect among groups.

Analyses of Terminal Field Volume and Density of Labels in Dorsal-Ventral Zones. The analyses of terminal field volumes and density here is the same as was done to study the role of *Bdnf* overexpression in the tongue on terminal field organization in the NST (Sun et al., 2015). The NST was subdivided into X, Y, and Z planes to help identify where terminal field organization of each nerve and the overlaps with other terminal fields occurred. For the medial-lateral and rostral-caudal analyses (X and Y), the NST in the horizontal plane was subdivided into uniform grid boxes of 100 pixels X 100 pixels. The grid was aligned relative to the NST, with the intersection of the most medial and most rostral borders of the NST as the 0,0 coordinate. The density of terminal field label was calculated in each grid box (100 X 100 pixels) for each physical section by dividing the respective terminal field volume within a grid box by the volume of the portion of the NST contained within the grid box (i.e., volume of terminal field label/volume of the NST within the grid box).

For analyses in the dorsal-ventral planes (Z), we examined the volume of labeled terminal field in four dorsal-ventral zones (see Sun et al., 2015 for details). The landmarks in controls and αENaC knockout mice were similar to that that described in Sun et al. (2015).

Measures of NST Volumes. The transmitted light images (4X) taken of all sections in control and in αENaC knockout mice were used to determine if the size of the NST differed between groups. The NST volume was measured using Neurolucida computer software (version 4.34; MicroBrightField). To calculate volume, the area measurements from all of the sections were summed and multiplied by 50 μm.

Statistical Analysis

Terminal Field Volumes. The mean ± SEM was calculated for the total CT, GSP, and IX nerve terminal field volumes, for their overlapping field volumes, and for terminal field volumes

within the four defined dorsal-ventral zones. Comparisons were made for the volume of each nerve and overlap between the control and αENaC knockout mice using independent samples t-tests. The Holm-Šídák step-down test was used to correct for multiple comparisons. We chose to start the step-down process with the unadjusted alpha level at 0.05 (Holm, 1979).

Density by Dorsal – Ventral Zones. Density measures were not statistically analyzed, but were qualitatively examined through heat maps for each dorsal-ventral zone containing a 5 X 10 (column X row) grid.

NST Volumes. The mean total NST volumes were compared between the two groups using an independent samples t-test.

Examination of Terminal Fields in Coronal Sections. The NST from 3 αENaC knockout and 3 control mice were sectioned coronally on a vibratome at 50μm and imaged as described above. Coronal sections were used to examine the extent of terminal field expansion and overlapping fields in the NST. No quantitative measurements were taken. Coronal sections were also imaged with transmitted light following confocal microscopy of the fluorescently labeled terminal fields to allow visualization of labeled chorda tympani nerve terminal fields in coronal sections.

Geniculate Ganglion and Petrosal Ganglion Cell Number. The CT (αENaC knockout, n=4; Controls, n=4) or the GSP (αENaC knockout, n=4; Controls, n=4) nerve was labeled as described for the terminal field labeling procedure, with the exception that the 3 kD tetramethylrhodamine dextran was chosen as the only tracer because it did not require further processing for visualization. After cardiac perfusion, geniculate ganglia were removed and post-fixed. Petrosal ganglia (αENaC knockout, n=4; Controls, n=4) were also labeled by way of the IX, using the tetramethylrhodamine tracer, and collected as described for the geniculate ganglia. Each intact ganglion was mounted on a slide and imaged on a scanning laser confocal

microscope. Serial 2μm optical sections were taken throughout each ganglion, as described previously in mouse (Shuler et al., 2004). Cell number was counted using Neurolucida computer software (version 4.34, MicroBrightField, Colchester, VT).

Statistical Analysis: Ganglion cell numbers were compared between αENaC knockout and control mice and analyzed using independent-samples T-tests. As noted in the statistical description for terminal field analyses, the Holm-Šídák step-down test was used to correct for multiple comparisons of ganglion cell numbers (i.e., cells of the CT, GSP and IX). We chose to start the step-down process with the unadjusted alpha level at 0.05 (Holm, 1979).

CT Nerve Neurophysiology. To establish that the knockout of the *Scnn1a* in the tongue resulted in reduced functional responses from the CT and GSP to NaCl at adulthood, (αENaC knockout, n=4; Controls, n=5) were anesthetized as described for the "Fluorescent Anterograde Nerve Labeling" procedure. The animals were tracheotomized and placed on a circulating water heating pad to maintain body temperature. Hypoglossal nerves were transected bilaterally to prevent tongue movement, and the mouse was placed in a nontraumatic head holder. The left CT was isolated using a mandibular approach. The nerve was exposed near the tympanic bulla, cut, desheathed, and positioned on a platinum electrode. A second electrode was placed in nearby muscle to serve as ground. Kwik-Sil was placed in the cavity around the nerve.

Functional taste responses were also recorded from the GSP in a αENaC knockout and in a control mouse. The neurophysiological procedure was followed as detailed by (Sollars and Hill, 1998; Sollars and Hill, 2000). Briefly, the heads of mice were held and stabilized by a non-traumatic headholder (Erickson, 1966) and placed in a supine position. The GSP was sectioned close to the geniculate ganglion and dissected free of underlying tissue. The nerve desheathed and positioned on a platinum electrode, with a reference electrode placed in nearby tissue.

Whole nerve CT or GSP activity was fed to a high impedance input stage amplifier and then led to a PowerLab A/D converter and amplifier and analyzed with PowerLab Scope software (ADInstruments, Mountain View, CA). Output of the PowerLab was fed to an audio monitor and to a computer monitor for monitoring activity.

Stimulation Procedure: All chemicals were reagent grade and prepared in artificial saliva (Hellekant et al., 1985). Neural responses from the CT were recorded to ascending concentrations series of 0.05, 0.1, 0.25, and 0.5 M NaCl, to 10, 20, and 50 mM citric acid, then to 0.1, 0.25, 0.5 and 1.0M sucrose, and finally to 10, 20, 50, and 100mM quinine hydrochloride to assess the taste responses to prototypical stimuli that represent salty, sour, sweet, and bitter, respectively, to humans. The concentration series to taste stimuli were similar to that used by Chandrashekar et al. (2010). Each concentration series was bracketed by applications of 0.5M NH_4Cl to monitor the stability of each preparation and for normalizing taste responses. Solutions were applied to the tongue in 5 ml aliquots with a syringe and allowed to remain to the tongue for ~20 sec. We used this period of stimulation so that we could ensure enough of a period to measure steady-state responses. After each solution application, the tongue was rinsed with artificial saliva for $\geq$1 min. This period allowed a full recovery of neural responses (i.e., the responses were not adapted by previous responses) (Shingai and Beidler, 1985). In addition, responses were recorded to the NaCl concentration series in the epithelial sodium channel blocker, amiloride (50 μM). Rinses during this series were to amiloride. Neural responses from the GSP were recorded only to an ascending concentrations series of 0.05, 0.1, 0.25, and 0.5 M NaCl before and after lingual application of amiloride.

CT and GSP responses were calculated as follows: the average voltage of the spontaneous activity that occurred for the second before stimulus onset was subtracted from the voltage that

occurred from the period from the first to sixth second after stimulus application. Response magnitudes were then expressed as ratios relative to the mean of 0.5M NH_4Cl responses before and after stimulation. Whole nerve response data were retained for analysis only when 0.5M NH_4Cl responses that bracketed a concentration series varied by <10%.

RESULTS

Scnn1a Expression was Significantly Decreased in αENaC Knockout *Mice.*

Expression of the *Scnn1a* gene in the tongue of αENaC knockout mice was 9% of that in controls at adulthood. The mean (± SEM) normalized expression ratio for controls was 1.05 (±0.04) and 0.09 (± 0.02) for αENaC knockout mice ($p < 0.0001$).

Neurophysiological Taste Responses to NaCl from the CT and GSP Were Decreased in αENaC Knockout *Mice.*

Conditionally deleting the *Scnn1a* gene in the taste buds throughout the oral cavity had profound and selective effects on CT taste responses. In αENaC knockout mice, increases in the concentration of NaCl as the taste stimulus did not increase the taste responses in the CT like that seen in control mice (Fig. 1A-D). For example, the relative responses of the CT to 0.1M, 0.25M and 0.5M NaCl in αENaC knockout mice were significantly less (40%-60%) than the respective responses in control mice ($p < 0.05$; Fig. 1E). Moreover, the epithelial sodium channel blocker, amiloride, had essentially no suppressive effect on NaCl taste responses in the CT of αENaC knockout mice, whereas, it significantly suppressed NaCl responses in controls to 0.1M, 0.25M and 0.5M NaCl ($p < 0.05$; Fig. 1E). In contrast to NaCl taste stimulation, responses of the CT to non-salt stimuli were similar between αENaC knockout and control mice throughout a concentration range for sucrose, citric acid, and quinine hydrochloride (Fig. 2). The type and

magnitude of the changes seen here for CT responses in αENaC knockout mice were similar to that reported by Chandrasekhar et al. (2010).

In rat, the GSP also responds robustly to taste stimulation with NaCl and that these responses are suppressed by amiloride (Sollars and Hill, 1998; Sollars and Hill, 2000). We show here that the GSP in a control mouse responds to NaCl similar to that in rat – relative response magnitudes increased with increasing NaCl concentration, such that the response magnitude to 0.5M NaCl and 0.5M NH_4Cl were similar and the responses were highly amiloride sensitive (Figs. 1F, G, J). By contrast, NaCl taste responses in the GSP of an αENaC knockout mouse failed to show the increase response to increasing NaCl concentrations and, like the CT in these mice, the responses were not significantly suppressed by amiloride (Fig. 1H, I, J). Therefore, both the CT and the GSP show profound functional deficits to NaCl stimulation.

Postnatal Body Weights Were Not Affected Removal of Scnn1a.

We now know that *Scnn1a* was selectively removed from taste buds in the mouth of αENaC knockout mice. However, since K19 is also expressed in the gut of mice (Brembeck et al., 2001), it is likely that *Scnn1a* was also removed in epithelial cells that transport NaCl (Duc et al., 1994; Chandrashekar et al., 2010).

To examine if removal of the *Scnn1a* gene had general, somatic effects on the development of αENaC knockout mice, we examine the body weights of αENaC knockout and control mice from P5 to P30 (αENaC knockout, n=16; control, n=20). We found that the mean body weights of αENaC knockout mice were at least 90% of control mice at P5, P10, P15, P20, P25 and P30, and that both groups followed the developmental body weight data shown for C57BL/6J mice from Jackson Laboratories (Bar Harbor, ME). Moreover, there were no apparent differences in

355 overall appearance, ingestive, or motor abilities. Similar observations of αENaC knockout mice
356 were reported by Chandrashekar et al. (2010).
357 In summary, the αENaC knockout mice used here are similar to those used to study peripheral
358 taste function in mice with the same genotype as ours (Chandrashekar et al., 2010), where it was
359 convincingly shown that sodium salt taste was selectively knocked out of the peripheral taste
360 system, yielding a taste modality specific loss of afferent information sent to the gustatory
361 brainstem.
362 *Removal of Scnn1a From Taste Buds Throughout Development Leads to Much Larger Terminal*
363 *Fields in the NST.*
364 Qualitative Appearance of Terminal Fields in Control and αENaC knockout mice.
365 Figure 3 shows the terminal fields of the IX, CT, GSP and the merged image of all terminal
366 fields in a control and in a αENaC knockout mouse for the 4 dorsal-ventral zones within the NST
367 described in the Methods. For all fields in all zones, the densest portion of the terminal field was
368 located in the rostral and medial portion of the NST. This is similar to that reported in rat (King
369 and Hill, 1991; May and Hill, 2006) and in mouse (Sun et al., 2015). For both groups, the
370 terminal fields extended more caudally in the Dorsal and Intermediate Zones compared to the Far
371 Dorsal and Ventral Zones (Fig. 3). Moreover, the IX terminal field seemed to occupy more of the
372 NST and with a higher density in the Far Dorsal, Dorsal, and Intermediate Zones than in the
373 Ventral Zone. By contrast, the CT and GSP terminal fields were located more ventrally than the
374 IX for both groups (Fig. 3). Figure 3 also illustrates that more label for all terminal fields
375 occurred in αENaC knockout mice compared to controls, especially in the Dorsal and
376 Intermediate Zones (Fig. 3). As a consequence of what appears to be more label in αENaC
377 knockout mice, there also seems to be more overlap among all three nerve terminal fields (Fig.

3D,H,L,P,T,X,BB,FF). The following sections describe the quantification data supporting these observations.

Measurements of Terminal Field Volumes.

Control mice. In control mice, the mean (± SEM) number of 50μm sections containing any terminal field label was 10.0 (± 0.4) sections, and the total terminal field volumes for the IX, CT and GSP were similar to each other (Fig. 4). The total terminal field volume of the overlap between the CT and the GSP was larger than the IX with GSP and IX with CT overlap volumes, which were similar to each other (Fig.4). This reflects the dorsal to ventral organization of the three fields within the NST, where the CT and GSP terminal fields are shifted slightly more ventral than the IX (see Figs. 3 and 4). As would be expected, the triple overlap among all three nerves was the smallest of all terminal fields.

αENaC knockout mice. The pattern of innervation of nerves and overlaps described for αENaC knockout mice was similar to that seen in control mice. However, the mean (± SEM) number of 50μm sections with terminal field label in αENaC knockout mice (11.7 ± 0.5) was significantly more ($p < 0.05$) than in controls. Moreover, the total terminal field volumes for all nerves and all overlapping fields in αENaC knockout mice were approximately 1.6X (GSP nerve) to 2.7X (IX with CT overlap) greater than that of the respective total terminal field volume in controls (Fig. 4). All of the αENaC knockout mice terminal field volumes were significantly greater than that in controls ($p < 0.05$). It is also important to see that the absolute volumes for the IX, CT, and GSP were very large in αENaC knockout mice compared to controls. For example, the mean CT terminal field volume in αENaC knockout mice was 75 X 10^5 μm^3 greater than controls.

The large size of terminal fields in αENaC knockout mice cannot be explained by a larger target (i.e., larger NST) compared to controls. Our analyses of the volume of the NST revealed that

401 there were no group-related differences. The mean NST volume (± SEM) for controls was 4.81
402 X 10^8 μm^3 (± .2) and 4.53 X 10^8 μm^3 (± .2) for αENaC knockout mice ($p = 0.33$).
403 *Expansion of the Terminal Fields and Differences in Terminal Field Densities Occur Primarily*
404 *in Dorsal and Intermediate Zones*. Knowing that large group-related differences existed in total
405 terminal field volumes, we wanted to know if these differences were localized to specific dorsal
406 to ventral zones. Moreover, we examined the regional distribution of terminal field labeling
407 through density measurements at each level to qualitatively examine the spatial organization of
408 the labels.
409 *Far Dorsal Zone*.
410 Volume:
411 *Control mice*: The amount of terminal field label in this dorsal-most zone contained the least
412 amount of label of all four zones in control mice -- all 7 control mice had label in this zone.
413 There was relatively more IX label in this zone compared with CT and GSP label (Fig. 5A). The
414 relatively low amounts of CT and GSP label resulted in correspondingly smaller amounts of
415 label where the nerves overlapped with other fields (Fig. 5A).
416 *αENaC knockout mice*: As seen in control mice, all mice in this group had label in the Far
417 Dorsal Zone and the number of sections in the zone did not differ between groups ($p > 0.05$).
418 Also, as found in control mice, there was relatively more IX label compared with CT and GSP
419 label, and relatively small amounts of overlapping terminal field labels (Fig. 5A). None of the
420 terminal field comparisons between controls and αENaC knockout mice were significantly
421 different ($p > 0.05$; Fig. 5A).
422 Density: The densities of label are depicted in the heat maps shown in Figure 5B, D, F, and H.
423 For brevity, we show only the heat maps for the three nerves (CT, GSP, IX), and the heat map

for the triple overlap (CT with GSP with IX). The heat maps for all three nerves and the overlaps for control and αENaC knockout mice were normalized to the grid box with the highest density label from the eight fields. For example, in the Far Dorsal Zone, the grid box with the highest density of label occurred for the IX label in αENaC knockout mice (see white rectangle in Fig. 5B). That value (122.7; total volume of terminal field label in a grid box/total volume for respective grid box X 10^3) was used as 100% intensity and all other density measures in this zone (volume of terminal field label/volume of the NST contained within the grid box X $10^3 \mu m^3$) were made relative to it (see heat map scale in Fig. 5B).

Control mice: As would be expected from the terminal field volume results for this zone (Fig. 5A), the terminal field distribution and densities were similar among the IX, CT, and GSP, with most of the label located towards the rostral pole of the NST. However, there was a trend for a more caudal spread of CT and GSP label compared to the IX (Fig. 5B).

αENaC knockout mice: The patterns of labels were similar between control and αENaC knockout mice for the three nerves and for the triple overlap of these nerves. However, there were higher terminal field densities for the IX than for the CT and GSP in αENaC knockout mice. Group-related differences in terminal field densities were most notable for the IX (Fig. 5B).

Dorsal Zone.

Volume:

Control mice. There was more terminal field label in this zone for the three nerves and areas of overlap compared to label seen in the Far Dorsal Zone (Fig. 5C). All control mice had label in this region. The IX label continued to be the most prevalent in this zone; however, significant amounts of CT and GSP label also occurred in the Dorsal Zone (Figs. 3 I-L; 5C). Moreover,

447 there were corresponding fields of overlap between two and among three nerve terminal fields
448 (Figs. 3L; 5C).
449 *αENaC knockout mice*. Similar to the label seen in the Far Dorsal Zone, there was more terminal
450 field label for IX than for CT then followed by GSP in this zone (Figs. 3M-P; 5C) in αENaC
451 knockout mice. This is a slightly different pattern than seen in control mice. Unlike the more
452 dorsal zone where there were no group-related significant differences, all of the terminal field
453 volumes were significantly greater than seen in control mice in this zone (Fig. 5C; $p < 0.05$). The
454 mean differences ranged from 71% to 350% greater for the GSP and triple overlap, respectively
455 (Fig. 5C).
456 Density:
457 *Control mice*. The shape of the IX label in control mice for the Dorsal Zone extended more
458 caudally and laterally in the NST than seen in the Far Dorsal Zone (Figs. 5B, D) and had the
459 greatest density of label compared to the other two nerves (Fig. 5D). By contrast, the shape of the
460 other terminal fields in controls were similar between the Far Dorsal and Dorsal Zones (Fig. 5B,
461 D).
462 *αENaC knockout mice*. Similar to the Far Dorsal Region, the grid box with the densest label was
463 for the IX label (white box in Fig. 5D). However, there were also regions of high density for the
464 CT in the NST of αENaC knockout mice, which was also qualitatively denser and expanded
465 more in the NST than in control mice (Fig. 5D). Similarly, the triple overlap of all three nerves in
466 αENaC knockout mice appears denser and extended more caudally and laterally compared to
467 control mice (Figs. 3P, 5D).
468 *Intermediate Zone*.
469 Volume:

Control mice. Unlike the two more dorsal zones in control mice, the CT and GSP made extensive projections into the Intermediate Zone, resulting in similar terminal field volumes among the three nerves (Fig. 5E). The projection of all three nerves to the Intermediate Zone also contributed to substantial amounts of overlapping fields among the three nerves, most notably the relatively large amount of overlap between the CT and GSP (Figs. 3T, 5E).

αENaC knockout mice. The three nerves also made extensive projections into this zone in αENaC knockout mice, with similar mean terminal field volumes. As noted for the Dorsal Zone, all of the terminal fields in αENaC knockout mice were significantly greater than that in control mice ($p < 0.05$; Fig. 5E). In this zone, the mean increase in terminal field volumes ranged from a 38% increase for the GSP to a 120% increase for the triple label compared to controls (Figs. 3X and 5E).

Density:

Control mice. There was nearly an identical pattern of density distribution for CT and GSP label in control mice, with the densest portions located primarily in the rostral and medial portion of the NST (Figs. 3 Q-T, 5F). This is reflected in densest regions of overlap among all three nerves (TRIPLE).

αENaC knockout mice. The densest grid box in this zone was for the CT label (Fig. 5F). This is unlike the more dorsal zones, where the IX label produced the densest projection. The pattern of labeling was similar between the CT, GSP, and the IX (also see triple overlap in Figs. 3T and 5F). While the location of the densest portion of the label was shared with control mice (i.e., rostral and medial NST), the label in αENaC knockout mice extended beyond that seen in control mice. The extension was primarily caudally and laterally for the IX, CT, GSP, and triple overlap (Figs. 3X and 5F).

493 *Ventral Zone*.

494 Volume:

495 *Control mice*. The ventral zone received substantially more CT and GSP label than IX in control
496 mice (Figs. 3 Y-BB; 5G). This was reflected in a relatively large proportion of CT and GSP label
497 overlap and small amount of overlap between IX with GSP and IX with CT, and a small amount
498 of overlap among all three nerves (Figs. 3BB; 5G).

499 *αENaC knockout mice*. The pattern of terminal field volume in αENaC knockout mice was
500 similar to that seen in control mice; however, the means for the CT, GSP, and CT with GSP
501 overlap were all greater than in αENaC knockout mice, but none were significantly different
502 from controls (Fig. 5G; $p > 0.05$). None of the other means were significantly different than in
503 control mice.

504 Density:

505 *Control mice*. The pattern and the densities in the Ventral Zone were very similar for the CT and
506 GSP in control mice, with dense regions of terminal field label in the rostral-medial portion of
507 the NST (Figs. 3Y-BB and 5H). The pattern of IX terminal field labeling was confined more to
508 the medial portion of the NST compared to the CT and GSP labels (see Fig. 5H).

509 *αENaC knockout mice*. Similar to the Intermediate Zone, the densest grid box for the Ventral
510 Zone occurred in the CT label (white box in Fig. 5H). As noted for the volume measurements,
511 where the means were very similar for the CT and GSP in αENaC knockout mice, the density
512 patterns were similar between these two nerves (Fig. 5H). Moreover, the density of label for the
513 CT and GSP was more of the lateral NST regions compared with control mice.

514 *Terminal Field Labeling Summary*. These results collectively show that there was a 60% to
515 300% greater terminal field volume in αENaC knockout mice compared to controls. We show

here that the terminal field volumes in αENaC knockout mice are not restricted to a single field, but occur in all terminal fields. A detailed density analysis of four dorsal-ventral zones of terminal field label revealed that the location of the densest label in the NST in each zone was similar between control and αENaC knockout mice, and the basic shapes of the terminal fields were similar between groups. However, the overall amount of label in each zone and the spread of label appears greater in αENaC knockout mice compared to controls, particularly in the Dorsal and Intermediate Zones.

Figure 6 shows a summary model of the terminal field organization of the IX, CT, and GSP in the Dorsal, Intermediate and Ventral Zones in horizontal sections for αENaC knockout mice and control mice. The figure depicts the relative terminal field volumes within an experimental group for each zone and the relative terminal field volume differences between groups.

Larger Terminal Fields in αENaC knockout mice are also seen in the Coronal Plane.

Figure 7 shows the terminal fields of the three nerves (A, C, E, Control IX, CT, GSP, respectively; B, D, F, αENaC knockout IX, CT, GSP, respectively) and their triple overlap (G, Control; H αENaC knockout)in the coronal plane. The section shown in the figure is from dorsal-caudal region of the NST (see Fig. 7I,J) to illustrate corresponding terminal field represented in the Dorsal Zone noted in Figures 3 and 5. From the label seen in these two animals, and confirmed in two additional animals in each group, the amount of CT and GSP terminal field labels in αENaC knockout mice extended more medially, laterally, and ventrally than in control mice (Fig. 7). This pattern is consistent with what is shown in Figures 5D and 5F. The pattern of innervation that we see with CT in coronal sections through the NST of control mice is similar to that shown in much more detail by others (Bartel and Finger, 2013; Ganchrow et al., 2014).

Ganglion Cell Numbers Are Not Affected by Deletion of the Scnn1a Gene .

A possible explanation for the group-related differences in terminal field size could be that more ganglion neurons survived to adulthood. That is, more ganglion cells in αENaC knockout mice could translate into a larger terminal field. To test this hypothesis, we counted the cell soma of the CT and GSP (geniculate ganglion) and of the IX (petrosal ganglion). There were no differences in IX, CT, or GSP mean numbers between αENaC knockout and control mice ($p > 0.05$). The mean (± SEM) ganglion cell number for the IX was 320 (± 11) for controls and 336 (± 33) for control and αENaC knockout mice, 197 (± 6) for controls and 201 (± 18) for the CT in controls and αENaC knockout mice, respectively, and 189 (± 3) for controls and 203 (± 18) for the GSP in controls and αENaC knockout mice, respectively.

DISCUSSION

Deletion of the gene responsible for αENaC in mouse taste buds during embryonic development and continuing through adulthood resulted in extensive expansion of the terminal fields of three nerves that carry gustatory information from the tongue to the NST. We show here that the terminal fields in αENaC knockout mice were expanded by as much as 3X compared to controls, resulting primarily from higher densities of label in the same terminal field areas as innervated in controls.

The gene deletion selectively disrupted sodium taste responses from the CT and GSP. Both nerves innervate taste bud cells that have αENaC and have been attributed to the discrimination of sodium salts from other salts and non-salt taste stimuli (Heck et al., 1984; Hill et al., 1990; Spector et al., 1996; Sollars and Hill, 1998). The selectivity of the functional effects to NaCl and the molecular data are consistent with those of Chandrasekhar et al. (2010), who first examined

561 the effects of deleting the gene for αENaC early in development on the peripheral gustatory
562 system.

563 *Terminal Field Effects of Targeted Gene Deletion of αENaC are Similar to Those in Life-Long*
564 *Dietary Sodium Restriction in Rats.*

565 One of the driving forces here in using mice with targeted deletions in the gene responsible for
566 αENaC was the ability to examine the role of a single taste modality (i.e., sodium salt taste) on
567 terminal field development with minimal (or the absence of) off-target effects. There was no
568 evidence that our αENaC knockout mice had gross developmental deficits. This is in contrast to
569 a rat model that we used previously, which yielded similar functional taste responses from the
570 CT and terminal field effects to what is reported here, but these experimental rats had severe
571 deficits in somatic growth that suggested nutritionally-related (i.e., non activity-dependent)
572 effects (May and Hill, 2006). Rats fed a sodium-restricted diet (0.03% NaCl) from 3 days
573 postconception, via their mothers, through adulthood showed selective sodium taste response
574 deficits in the CT and enlarged terminal fields of the CT and IX in the NST at adulthood (Hill et
575 al., 1986; Hill, 1987; May and Hill, 2006; Sollars et al., 2006). Interestingly, there were no
576 group-related differences in GSP terminal field size in the sodium-restricted rats (Sollars and
577 Hill, 2000). This lack of terminal field change in sodium-restricted rats can be predicted from
578 functional data because the amiloride-sensitive NaCl response from the GSP in the experimental
579 rats was not affected by the low sodium diet (Sollars and Hill, 2000). Thus, there are striking
580 similarities between these two experimental manipulations -- decreased taste responses to NaCl
581 in the respective nerves (i.e., salt taste-elicited taste activity) were associated with expanded
582 terminal fields. The exception to this relationship is the finding that relates to the large IX
583 terminal field in life-long sodium-restricted rats and in αENaC knockout mice. In both cases, the

584 IX terminal field was at least 2X that of controls, yet it is highly unlikely that there is a
585 significant alteration in sodium-salt taste responses in either species because the IX is relatively
586 poorly responsive to NaCl and not suppressed by amiloride (Formaker and Hill, 1988; Ninomiya
587 et al., 1991; Ninomiya, 1998). Importantly, Chandrasekhar et al. (2010) also showed a lack of the
588 appropriate subunit composition of the ENaC channel in posterior taste buds to transduce the
589 amiloride component of the NaCl taste response in both knockout and control mice.

590 *Enlarged Terminal Fields May Relate to a Failure to "Prune" Exuberant Axonal Arbors.*

591 One of the hallmarks of circuit development in mammalian sensory systems is that central
592 terminal fields are large during early development and exuberant arbors are then eliminated, or
593 "pruned" during a period of postnatal circuit refinement (Katz and Shatz, 1996; Chen and
594 Regehr, 2000; Hooks and Chen, 2006; Ziburkus and Guido, 2006). In the rat gustatory system,
595 the terminal fields of the CT, GSP and IX are large, extensively occupy the rostral and
596 intermediate regions of the NST, and have overlapping territory with each other at postnatal day
597 15 (P15) (Mangold and Hill, 2008). All three fields then decrease by up to 3 fold from postnatal
598 day 15 to 35, when they take on their adult terminal field characteristics (Mangold and Hill,
599 2008). We recently found a similar development of these three terminal fields in the developing
600 C57BL/6J mouse (Zheng et al., 2014). Importantly, in both species, the dynamic phase of
601 terminal field "pruning" roughly coincides in age with a three-fold increase in relative taste
602 response magnitudes of the CT to NaCl (Hill and Almli, 1980; Yamada, 1980; Ferrell et al.,
603 1981; Hill and Bour, 1985; Zheng et al., 2014).

604 We also noticed here that the terminal field in adult αENaC knockout mice has the appearance of
605 terminal fields seen in of young, control mice – large terminal fields that overlap extensively
606 with the fields of other nerves. This suggests that mechanisms involved in "pruning" terminal

607 fields were not operational during development of the αENaC knockout mice. Assuming a
608 reliance of circuit refinement on the presence of neural activity, a decrease or absence of sodium
609 salt taste responses during this critical period may be instrumental in the failure to "prune"
610 exuberant arbors and synapses. We propose that salt taste stimulation supplied by salivary
611 sodium as well as in the milk and chow provides the necessary neural activity to drive age-
612 related "pruning" in controls, but is lacking in knockout mice.
613 The lack of sodium salt-elicited taste responses in the GSP would also be expected to yield the
614 observed large terminal fields in αENaC knockout mice. However, as noted earlier, taste
615 responses in the IX should not have been altered in αENaC knockout mice. Thus, the hypothesis
616 that taste-elicited activity should drive "pruning" of the terminal fields does not seem to follow
617 for the IX. Multiple factors may account for these results. One may be that the spontaneous
618 activity (e.g., elicited through salivary sodium) of the IX could be reduced in αENaC knockout
619 mice, resulting in a sustained decrease in neural activity, independent of taste-elicited activity. A
620 second possibility is that experimentally-induced alterations in one or more terminal fields
621 induce changes in other nerve terminal fields. Indeed, there is evidence that the three terminal
622 fields compete with each to ultimately shape terminal field organization in the rostral NST
623 (Corson and Hill, 2011), and that changes in neurotrophic factors (e.g., BDNF) in the NST
624 induced by one nerve may alter neighboring terminal fields (Sun et al., 2015). While we do not
625 know the precise dynamics of this process(es), our findings here indicate that the large terminal
626 field of the IX in knockout mice could be influenced by the lack of "pruning" by the other two
627 nerve terminal fields (i.e., CT and GSP).
628 *The Rodent Retinogeniculate Visual System – A Potential Model for Gustatory Terminal Field*
629 *Development*

Extensive work on the role of neuronal activity in shaping the mammalian development of sensory nerve terminal fields likely comes from work in the visual system, particularly in the dorsal lateral geniculate nucleus (dLGN). Before eye opening, projections of the retinal ganglion cells to the dLGN segregate into eye-specific layers through a process involving intrinsic, correlated, spontaneous activity in the two retinae, and not driven by stimuli in the visual world (Katz and Shatz, 1996; Hooks and Chen, 2006). These connections are then refined from about the age of eye opening, where spontaneous activity of the optic nerve continues to play a critical role, through an extended postnatal period where synapses are competitively eliminated or maintained by visually-evoked responses (Sretavan and Shatz, 1984; Katz and Shatz, 1996; Chen and Regehr, 2000; Hooks and Chen, 2006; Ziburkus and Guido, 2006). Not all of retinogeniculate development is due to neuronal activity because early projecting retinal ganglion cells are directed topographically to the LGN through chemical gradients (Pfeiffenberger et al., 2005). Nonetheless, it is clear that early "intrinsic" activity programs and later occurring, visually-guided processes shape and maintain the terminal fields of both optic nerves.

We suggest that a similar sequence of processes operates in the development of terminal fields in the rodent NST. Chemical guidance cues likely direct the "gustatory nerves" to the rostral and intermediate areas of the NST, where they overlap extensively with each other during embryonic and early postnatal development (Zhang and Ashwell, 2001). Then, with the onset and subsequent development of taste-elicited activity, the large terminal fields are "pruned" extensively to their mature size and location. Disruption of at least the taste activity-dependent process through a lack of one or more taste signals (e.g., salt taste) during development maintains terminal fields with an immature organization. Unanswered questions remain from this work

653 concerning whether the expanded field in knockout mice makes functional synapses, if there are
654 significant postsynaptic changes in structure and function, and what role changes in circuitry that
655 we describe here have on taste-elicited and ingestive behaviors.

REFERENCES

Bartel DL, Finger TE (2013) Reactive microglia after taste nerve injury: comparison to nerve injury models of chronic pain. F1000Research 2:65.

Brembeck FH, Moffett J, Wang TC, Rustgi AK (2001) The keratin 19 promoter is potent for cell-specific targeting of genes in transgenic mice. Gastroenterology 120:1720-1728.

Chandrashekar J, Kuhn C, Oka Y, Yarmolinsky DA, Hummler E, Ryba NJ, Zuker CS (2010) The cells and peripheral representation of sodium taste in mice. Nature 464:297-301.

Chen C, Regehr WG (2000) Developmental remodeling of the retinogeniculate synapse. Neuron 28:955-966.

Corson SL, Hill DL (2011) Chorda tympani nerve terminal field maturation and maintenance is severely altered following changes to gustatory nerve input to the nucleus of the solitary tract. J Neurosci 31:7591-7603.

Davis BJ (1988) Computer-generated rotation analyses reveal a key three-dimensional feature of the nucleus of the solitary tract. Brain Res Bull 20:545-548.

Duc C, Farman N, Canessa CM, Bonvalet JP, Rossier BC (1994) Cell-specific expression of epithelial sodium channel alpha, beta, and gamma subunits in aldosterone-responsive epithelia from the rat: localization by in situ hybridization and immunocytochemistry. J Cell Biol 127:1907-1921.

Erickson RP (1966) Nontraumatic headholder for rats. Physiol Behav 1:97-98.

Ferrell MF, Mistretta CM, Bradley RM (1981) Development of chorda tympani taste responses in rat. Journal of Comparative Neurology 198:37-44.

Formaker BK, Hill DL (1988) An analysis of residual NaCl taste response after amiloride. Am J Physiol 255:R1002-1007.

681 Ganchrow D, Ganchrow JR, Cicchini V, Bartel DL, Kaufman D, Girard D, Whitehead MC
682 (2014) Nucleus of the solitary tract in the C57BL/6J mouse: Subnuclear parcellation,
683 chorda tympani nerve projections, and brainstem connections. J Comp Neurol 522:1565-
684 1596.
685 Heck GL, Mierson S, DeSimone JA (1984) Salt taste transduction occurs through an amiloride-
686 sensitive sodium transport pathway. Science 223:403-405.
687 Hellekant G, af Segerstad CH, Roberts T, van der Wel H, Brouwer JN, Glaser D, Haynes R,
688 Eichberg JW (1985) Effects of gymnemic acid on the chorda tympani proper nerve
689 responses to sweet, sour, salty and bitter taste stimuli in the chimpanzee. Acta Physiol
690 Scand 124:399-408.
691 Hill DL (1987) Susceptibility of the developing rat gustatory system to the physiological effects
692 of dietary sodium deprivation. J Physiol (Lond) 393:413-424.
693 Hill DL, Almli CR (1980) Ontogeny of chorda tympani nerve responses to gustatory stimuli in
694 the rat. Brain Res 197:27-38.
695 Hill DL, Bour TC (1985) Addition of functional amiloride-sensitive components to the receptor
696 membrane: a possible mechanism for altered taste responses during development. Brain
697 Res 352:310-313.
698 Hill DL, Mistretta CM, Bradley RM (1986) Effects of dietary NaCl deprivation during early
699 development on behavioral and neurophysiological taste responses. Behav Neurosci
700 100:390-398.
701 Hill DL, Formaker BK, White KS (1990) Perceptual characteristics of the amiloride-suppressed
702 sodium chloride taste response in the rat. Behav Neurosci 104:734-741.

703 Holm S (1979) A simple sequentially rejective multiple test procedure. Scandinavian Journal of
704 Statistics 6:65-70.
705 Hooks BM, Chen C (2006) Distinct roles for spontaneous and visual activity in remodeling of
706 the retinogeniculate synapse. Neuron 52:281-291.
707 Huang T, Krimm RF (2010) Developmental expression of Bdnf, Ntf4/5, and TrkB in the mouse
708 peripheral taste system. Dev Dyn 239:2637-2646.
709 Hubel DH, Wiesel TN (1962) Receptive fields, binocular interaction and functional architecture
710 in the cat's visual cortex. J Physiol 160:106-154.
711 Hummler E, Merillat AM, Rubera I, Rossier BC, Beermann F (2002) Conditional gene targeting
712 of the Scnn1a (alphaENaC) gene locus. Genesis 32:169-172.
713 Katz LC, Shatz CJ (1996) Synaptic activity and the construction of cortical circuits. Science
714 274:1133-1138.
715 King CT, Hill DL (1991) Dietary sodium chloride deprivation throughout development
716 selectively influences the terminal field organization of gustatory afferent fibers
717 projecting to the rat nucleus of the solitary tract. J Comp Neurol 303:159-169.
718 Lasiter PS, Wong DM, Kachele DL (1989) Postnatal development of the rostral solitary nucleus
719 in rat: dendritic morphology and mitochondrial enzyme activity. Brain Res Bull 22:313-
720 321.
721 Mangold JE, Hill DL (2008) Postnatal reorganization of primary afferent terminal fields in the
722 rat gustatory brainstem is determined by prenatal dietary history. J Comp Neurol
723 509:594-607.

May OL, Hill DL (2006) Gustatory terminal field organization and developmental plasticity in the nucleus of the solitary tract revealed through triple-fluorescence labeling. J Comp Neurol 497:658-669.

Mistretta CM, Hill DL (2003) Development of the Taste System: Basic Neurobiology. In: Handbook of Olfaction and Gustation (Doty RL, ed), pp 759-782. New York: Marcel Dekker.

Ninomiya Y (1998) Reinnervation of cross-regenerated gustatory nerve fibers into amiloride-sensitive and amiloride-insensitive taste receptor cells. Proc Natl Acad Sci U S A 95:5347-5350.

Ninomiya Y, Tanimukai T, Yoshida S, Funakoshi M (1991) Gustatory neural responses in preweanling mice. Physiol Behav 49:913-918.

Pfeiffenberger C, Cutforth T, Woods G, Yamada J, Renteria RC, Copenhagen DR, Flanagan JG, Feldheim DA (2005) Ephrin-As and neural activity are required for eye-specific patterning during retinogeniculate mapping. Nat Neurosci 8:1022-1027.

Ridler TW, Calvard S (1978) Picture Thresholding Using an Iterative Selection Method. Ieee T Syst Man Cyb 8:630-632.

Shingai T, Beidler LM (1985) Response characteristics of three taste nerves in mice. Brain Res 335:245-249.

Shuler MG, Krimm RF, Hill DL (2004) Neuron/target plasticity in the peripheral gustatory system. J Comp Neurol 472:183-192.

Sollars SI, Hill DL (1998) Taste responses in the greater superficial petrosal nerve: substantial sodium salt and amiloride sensitivies demonstrated in two rat strains. Behav Neurosci 112:991-1000.

747 Sollars SI, Hill DL (2000) Lack of functional and morphological susceptibility of the greater
748 superficial petrosal nerve to developmental dietary sodium restriction. Chem Senses
749 25:719-727.
750 Sollars SI, Walker BR, Thaw AK, Hill DL (2006) Age-related decrease of the chorda tympani
751 nerve terminal field in the nucleus of the solitary tract is prevented by dietary sodium
752 restriction during development. Neuroscience 137:1229-1236.
753 Spector AC, Travers SP (2005) The representation of taste quality in the mammalian nervous
754 system. Behav Cogn Neurosci Rev 4:143-191.
755 Spector AC, Glendinning JI (2009) Linking peripheral taste processes to behavior. Curr Opin
756 Neurobiol 19:370-377.
757 Spector AC, Guagliardo NA, St John SJ (1996) Amiloride disrupts NaCl versus KCl
758 discrimination performance: implications for salt taste coding in rats. J Neurosci 16:8115-
759 8122.
760 Sretavan D, Shatz CJ (1984) Prenatal development of individual retinogeniculate axons during
761 the period of segregation. Nature 308:845-848.
762 Sun C, Dayal A, Hill DL (2015) Expanded terminal fields of gustatory nerves accompany
763 embryonic BDNF overexpression in mouse oral epithelia. J Neurosci 35:409-421.
764 Vogt MB, Hill DL (1993) Enduring alterations in neurophysiological taste responses after early
765 dietary sodium deprivation. J Neurophysiol 69:832-841.
766 Whitehead MC (1988) Neuronal architecture of the nucleus of the solitary tract in the hamster. J
767 Comp Neurol 276:547-572.
768 Yamada T (1980) Chorda tympani resonses to gustatory stimuli in developing rats. Japanese
769 Journal of Physiology 30:631-643.

770 Zhang LL, Ashwell KW (2001) The development of cranial nerve and visceral afferents to the
771 nucleus of the solitary tract in the rat. Anat Embryol (Berl) 204:135-151.
772 Zheng S, Sun C, Hill D (2014) Postnatal reorganization of primary gustatory afferent terminal
773 fields in the mouse brainstem is altered by prenatal dietary sodium history. ABSTRACT
774 Society for Neurosciences.
775 Ziburkus J, Guido W (2006) Loss of binocular responses and reduced retinal convergence during
776 the period of retinogeniculate axon segregation. Journal of Neurophysiology 96:2775-
777 2784.
778

779 **LEGENDS**

780 **Figure 1. A.** Integrated taste responses from the chorda tympani nerve (CT) in a control
781 (Control) mouse to a concentration series of NaCl and to 0.5M NH_4Cl before lingual application
782 of the epithelial channel blocker, amiloride, and **B.** with amiloride. **C.** Integrated taste responses
783 from the CT in an αENaC knockout (KO) mouse to a concentration series of NaCl and to 0.5M
784 NH_4Cl before lingual application of amiloride and **D.** with amiloride. **E.** Mean (± SEM) relative
785 taste responses to a concentration of NaCl from the CT in control and αENaC knockout (KO)
786 mice before (solid lines) and with lingual application of amiloride (dotted lines). **F.** Integrated
787 taste responses from the greater superficial petrosal (GSP) in a control (Control) mouse to a
788 concentration series of NaCl and to 0.5M NH_4Cl before lingual application of amiloride, and **G.**
789 with amiloride. **H.** Integrated taste responses from the GSP in an αENaC knockout (KO) mouse
790 to a concentration series of NaCl and to 0.5M NH_4Cl before lingual application of amiloride and
791 **I.** with amiloride. The record in I is broken to enable registration of responses with G. Only
792 spontaneous activity was not shown in I. **J.** Relative taste responses to a concentration of NaCl
793 from the GSP in the same control mouse in which F and G were recorded and in the same
794 αENaC knockout (KO) mouse in which H and I were recorded before (solid lines) and with
795 lingual application of amiloride (dotted lines). Asterisks denote $p < 0.05$ in the group-related
796 comparisons in **E.**

797 **Figure 2.** Mean (± SEM) relative taste responses to a concentration of **A.** sucrose, **B.** citric acid,
798 and **C.** quinine from the CT in control (Control; solid lines) and αENaC knockout (KO; dotted
799 lines).

800 **Figure 3.** Horizontal sections of labeled terminal fields of the glossopharyngeal (IX, green;
801 A,E,I,M,Q,U,Y,CC), chorda tympani (CT, blue; B,F,J,N,R,V,Z,DD), and greater superficial

802 petrosal (GSP, red; C,G,K,O,S,W,AA,EE) nerves and for the merged images of all three nerves
803 (MERGE, D,H,L,P,T,X,BB,FF) for control (Control; A-D, I-L, Q-T,Y-BB) and αENaC
804 knockout (KO; E-H, M-P, U-X, CC-FF) mice in the Far Dorsal (A-H), Dorsal (I–P),
805 Intermediate (Q-X) zones, and Ventral (Y-FF) within the mouse NST. The approximate location
806 of the NST is outlined in white, as shown in the merged images. The CT-GSP overlap is shown
807 as magenta, the IX-GSP overlap is shown as yellow, the IX-CT overlap in shown as blue-green,
808 and the CT-GSP-IX terminal field overlap is shown as white. Refer to the color guide in F. Scale
809 bar shown in G, 200 μm. R, Rostral; L, lateral shown in E.
810 **Figure 4.** Mean (±SEM) total terminal field volumes of the terminal field for the IX, CT, and
811 GSP nerves and their double and triple overlap of terminal fields in control (Control, open bars)
812 and αENaC knockout (KO; solid bars) mice. Asterisk denotes $p<0.05$.
813 **Figure 5.** Mean (± SEM) terminal field volumes and densities in x, y, and z planes in control
814 (Control; open bars) and αENaC knockout (KO; solid bars) mice. **A, C, E, G**, Mean (± SEM)
815 terminal field volumes of the glossopharyngeal (IX), chorda tympani (CT), and greater
816 superficial petrosal (GSP) nerves and their overlapping fields for (Control; open bars) and
817 αENaC knockout (KO; solid bars) mice in the Far Dorsal (A), Dorsal (C), Intermediate (E), and
818 Ventral (G) zones. Note the different Y axis in A. Asterisks shown for terminal field volumes
819 denote KO means significantly greater than in Control mice ($p<0.05$). **B, D, F, H**, Heat maps
820 showing the terminal field densities (volume of terminal field label in a division/total volume of
821 the division) for IX, CT, and GSP nerves, and for the triple overlap of all three nerve terminal
822 fields (TRIPLE). The NST (borders shown in white) has been rotated so that the solitary tract is
823 oriented vertically (see Methods section and see R, rostral, and L, lateral orientations in B,
824 TRIPLE overlap). The NST for each zone is divided into a maximum of 100 X 100 pixel

825 divisions for each optical image (see Methods). The colors for the heat map of densities are on
826 the relative scale shown in B, with 0% of maximum density noted as dark blue and 100% noted
827 as red. This relative scale was applied to each of the four zones; therefore, the maximum density
828 was obtained from all of the divisions from Control and αENaC knockout mice for the Far
829 Dorsal Zone, and similarly for the Dorsal, Intermediate and Ventral Zones. The division
830 representing 100% (brightest red) in B, D, F, and H are shown by a white border around the
831 respective 100 X 100 pixel division (e.g., contained in the IX terminal field of αENaC knockout
832 mice in the Far Dorsal Zone).

833 **Figure 6.** Schematic of the terminal field organization in the NST in control (Control; left
834 column) mice and αENaC knockout (KO; right column) mice for the Dorsal, Intermediate and
835 Ventral Zones. For comparisons, the total volume of terminal field of the Far Dorsal and Dorsal
836 Zones were summed and represented here as the "Dorsal Zone". The size of the terminal fields
837 was calculated relative to the terminal field volume for the glossopharyngeal nerve in the control
838 mouse (IX; hatched green oval in Dorsal Zone; area = 1.0). The color of individual nerves and of
839 their overlaps are shown in the color wheel and the orientation of the ovals are shown as they
840 appear in horizontal sections. R – Rostral; L – Lateral.

841 **Figure 7.** Coronal sections through the dorsal/caudal NST showing the IX terminal field (green;
842 A,B), CT terminal field (blue, C,D), GSP terminal field (red, E,F), merged (G,H) terminal fields,
843 and the terminal fields in the right hemifield of medulla captured with transmitted light (I, J) in
844 control (Control; A,C,E,G,I) and αENaC knockout (KO; B,D,F,H,J) mice. The orientation of the
845 sections is shown in G; D, Dorsal, L, Lateral. The color bar for the merged images in shown in
846 H. Scale bar in A = 200μm. Scale bar in J = 500μm. The black lines shown in I and J demarcate
847 the NST (thicker lines) and structures within the NST (thinner lines). 4V, 4^{th} ventricle; 12,

848 hypoglossal nuclei; 10, dorsal motor nucleus of the vagus; Cu, cuneate nucleus; ECu, external
849 cuneate nucleus; Sol, solitary tract; SolIM, solitary tract nucleus, intermediate; SolDL, solitary
850 tract, dorsolateral. Black, straight lines in I and J point to the relevant structure in the NST.

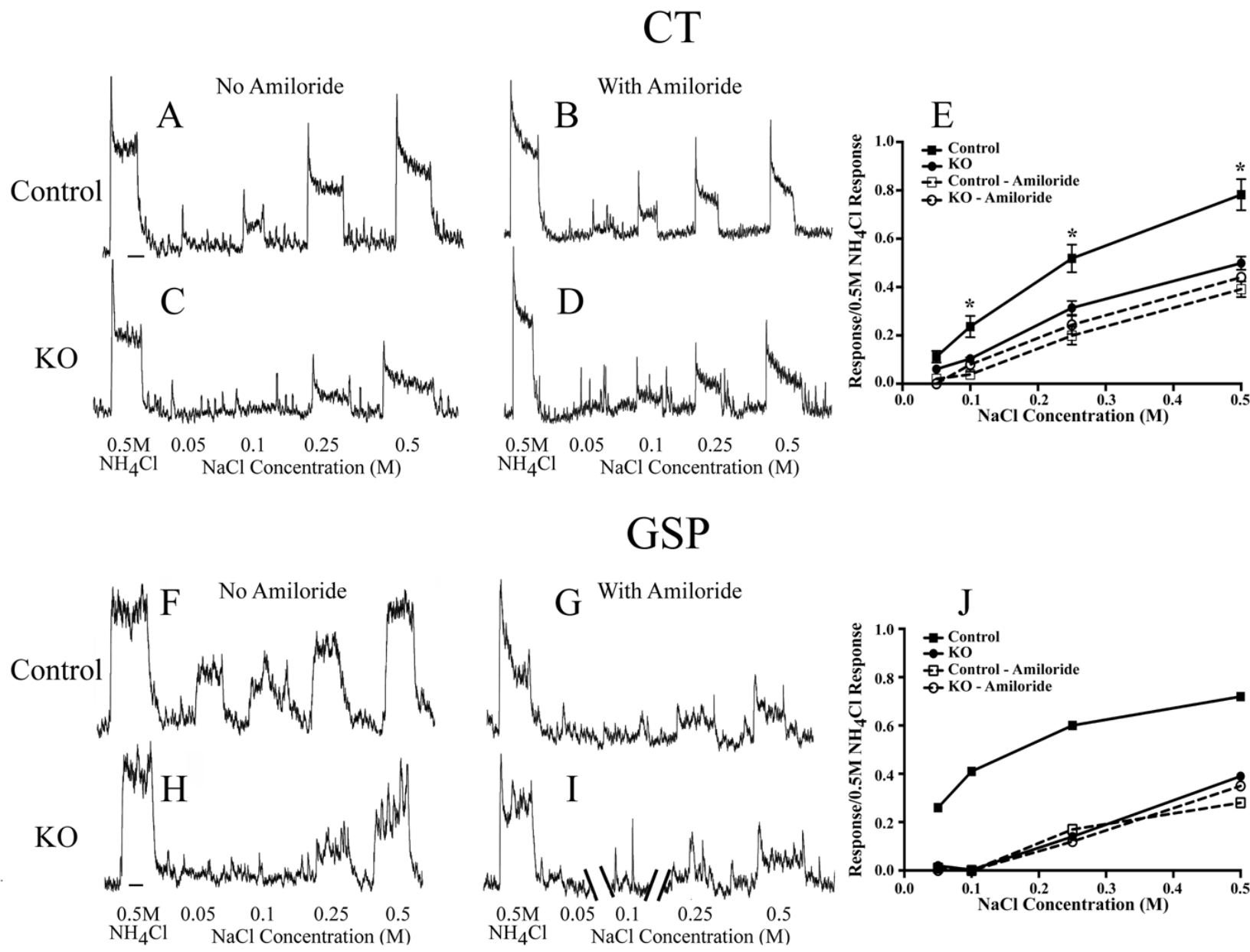
CT
No Amiloride
With Amiloride
A
B
C
D
E
Control
KO
0.5M NH4Cl
0.05
0.1
0.25
0.5
NaCl Concentration (M)
Control
KO
Control - Amiloride
KO - Amiloride
Response/0.5M NH4Cl Response
NaCl Concentration (M)
GSP
F
G
H
I
J

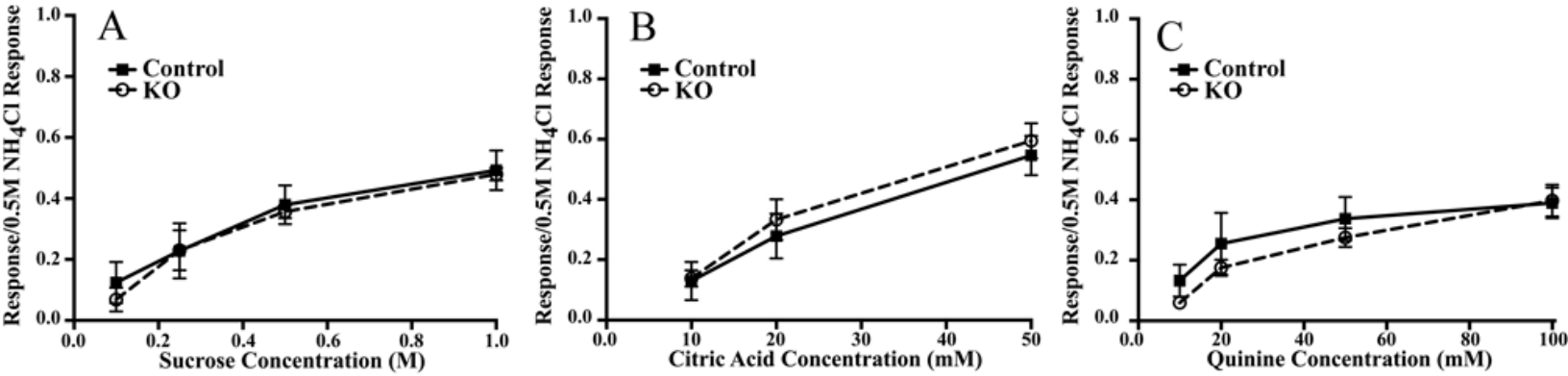
A
Control
KO
Response/0.5M NH4Cl Response
Sucrose Concentration (M)
B
Control
KO
Response/0.5M NH4Cl Response
Citric Acid Concentration (mM)
C
Control
KO
Response/0.5M NH4Cl Response
Quinine Concentration (mM)

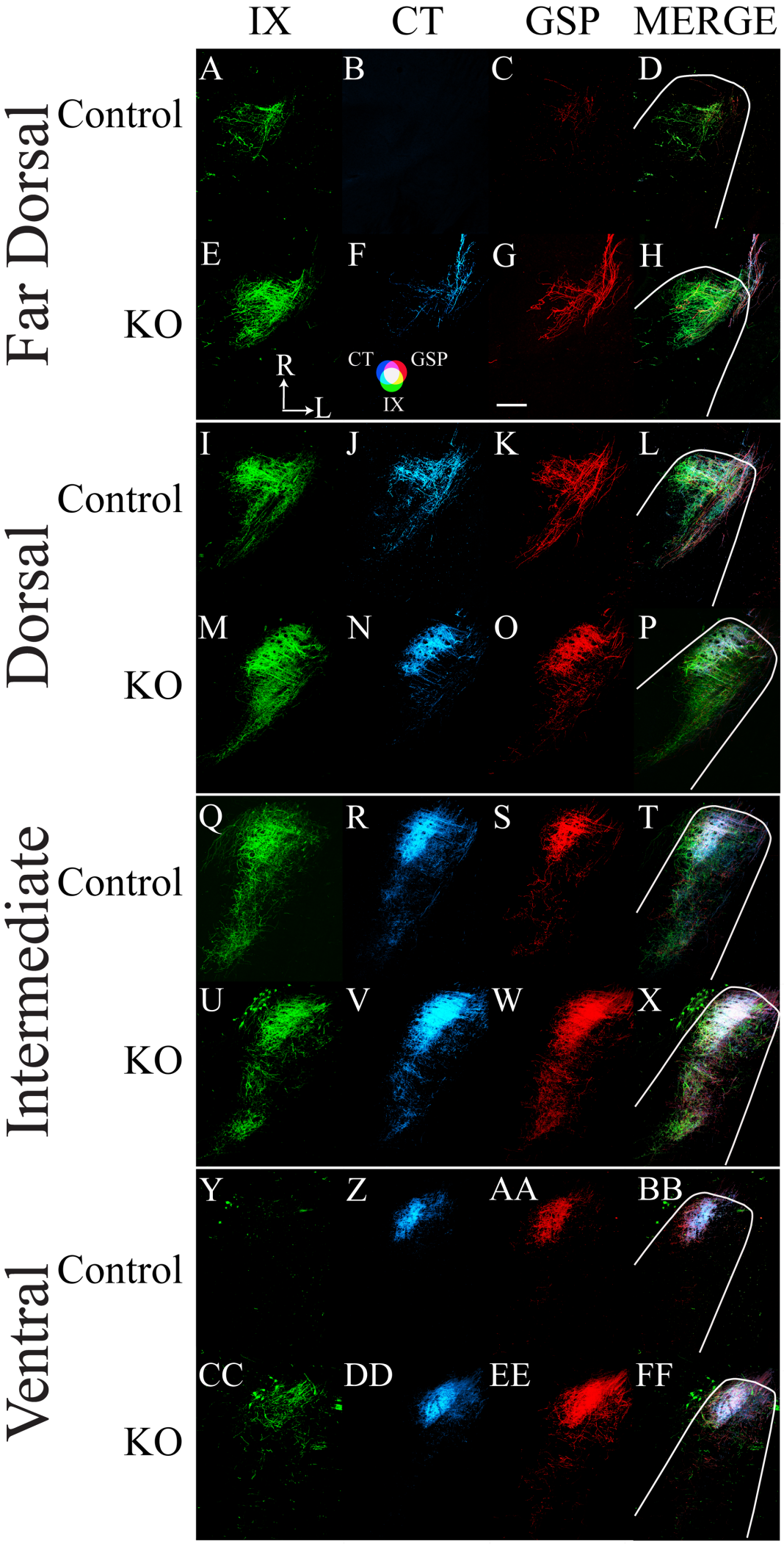
IX
CT
GSP
MERGE
Far Dorsal
Control
KO
Dorsal
Control
KO
Intermediate
Control
KO
Ventral
Control
KO
A
B
C
D
E
F
G
H
I
J
K
L
M
N
O
P
Q
R
S
T
U
V
W
X
Y
Z
AA
BB
CC
DD
EE
FF
R
L
CT
GSP
IX

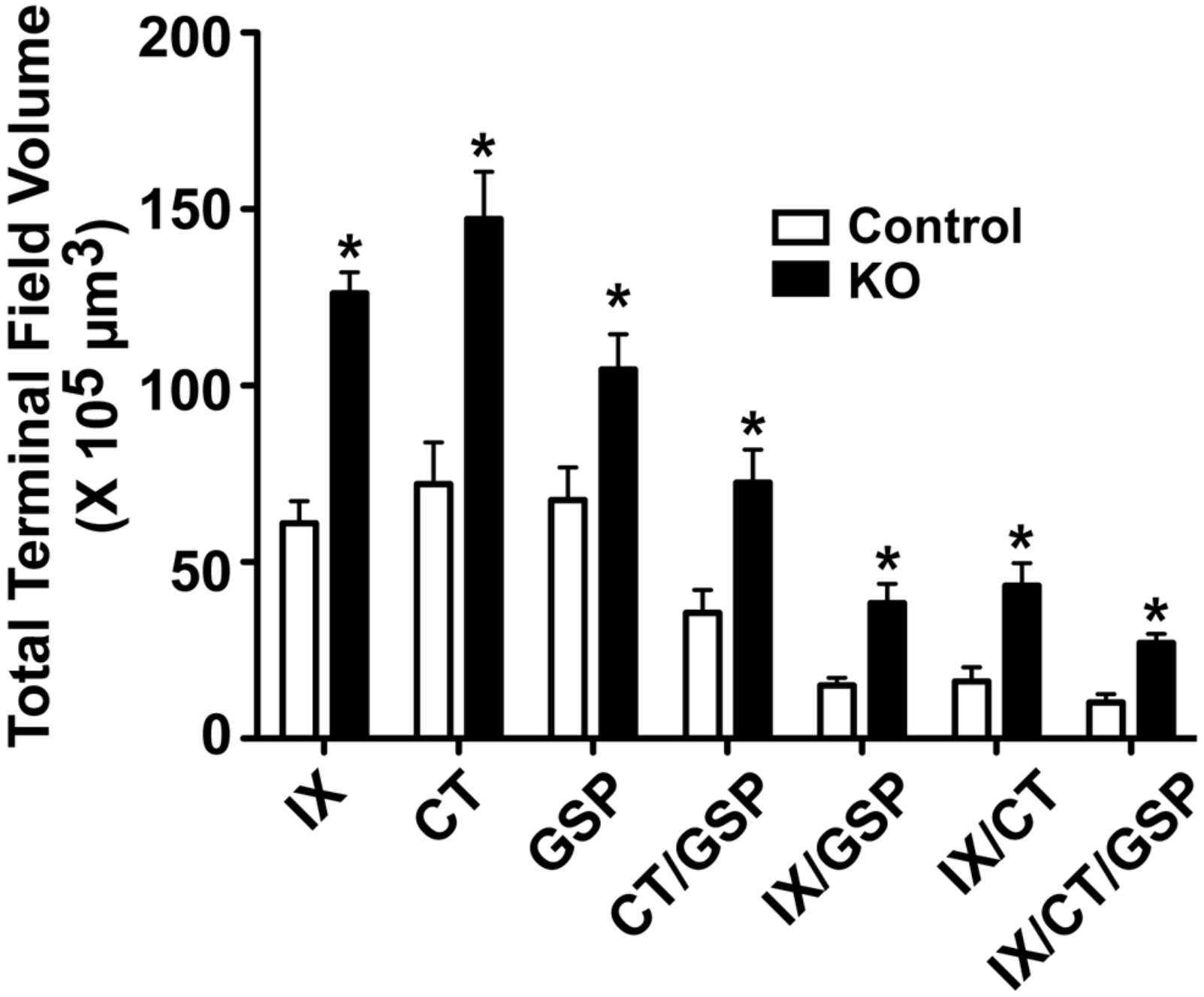
Total Terminal Field Volume
(X 10^5 µm^3)
200
150
100
50
0
Control
KO
*
IX
CT
GSP
CT/GSP
IX/GSP
IX/CT
IX/CT/GSP

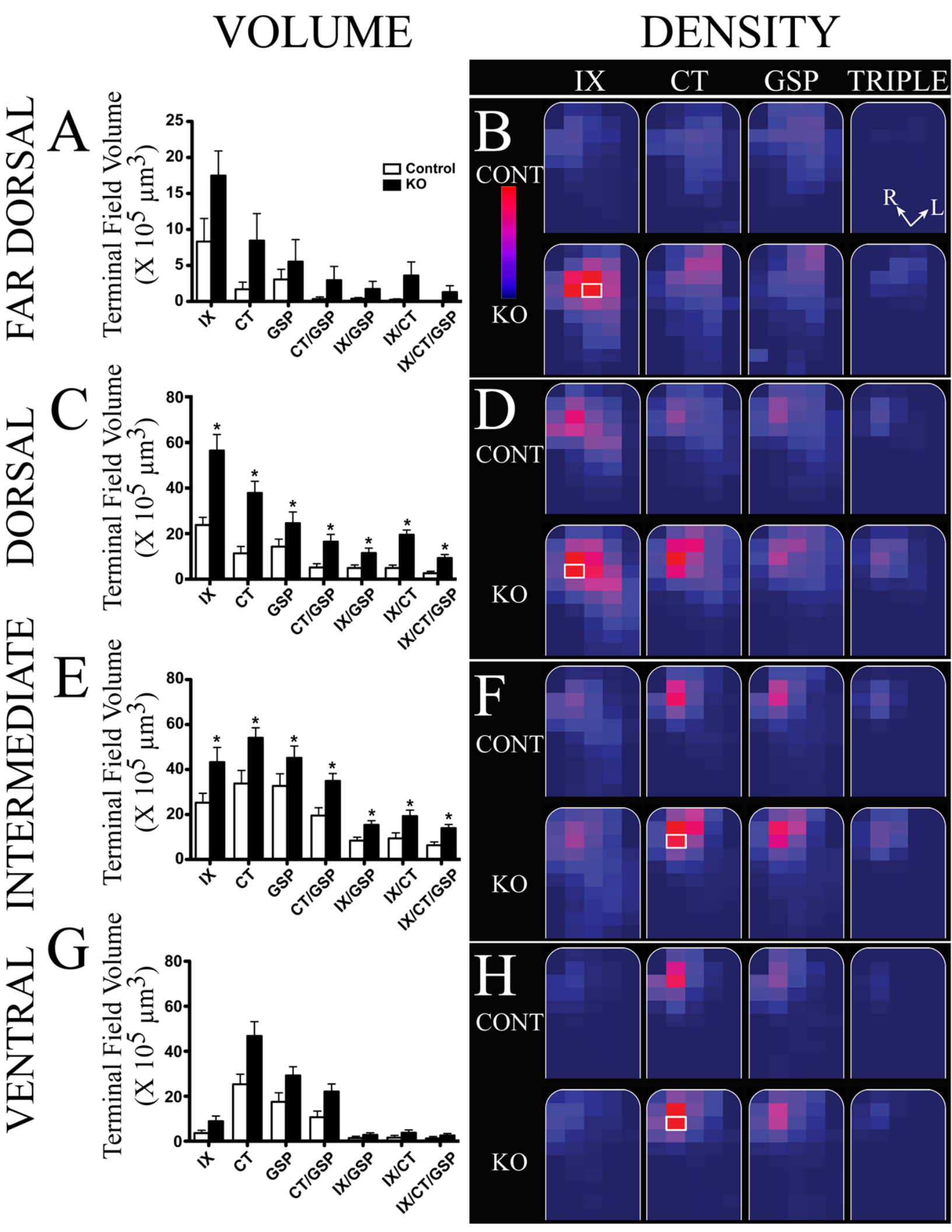
VOLUME
DENSITY
IX
CT
GSP
TRIPLE
FAR DORSAL
DORSAL
INTERMEDIATE
VENTRAL
A
B
C
D
E
F
G
H
CONT
KO
R
L
Control
KO
Terminal Field Volume
(X 10^5 µm^3)
IX
CT
GSP
CT/GSP
IX/GSP
IX/CT
IX/CT/GSP

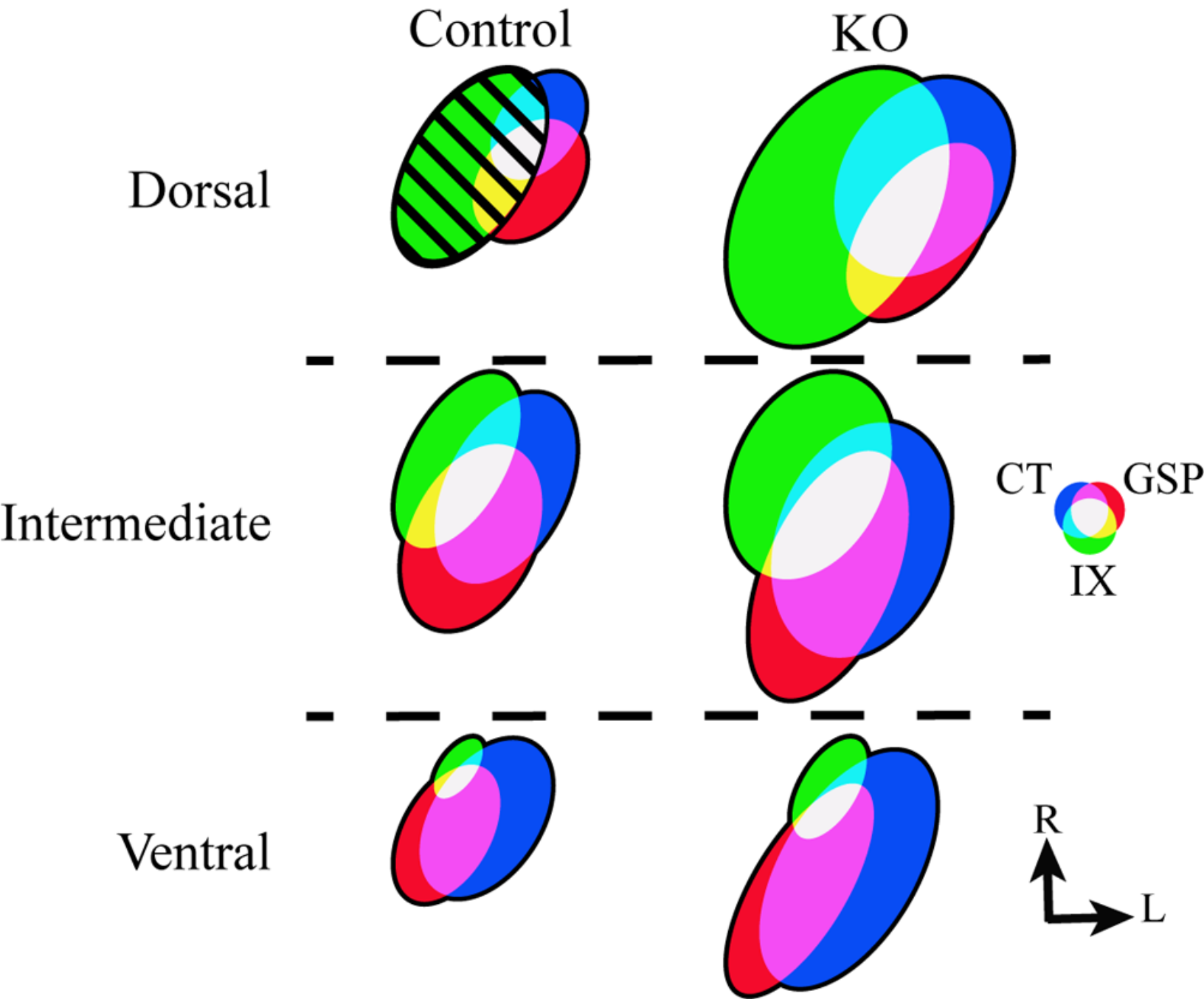
Control
KO
Dorsal
Intermediate
Ventral
CT
GSP
IX
R
L

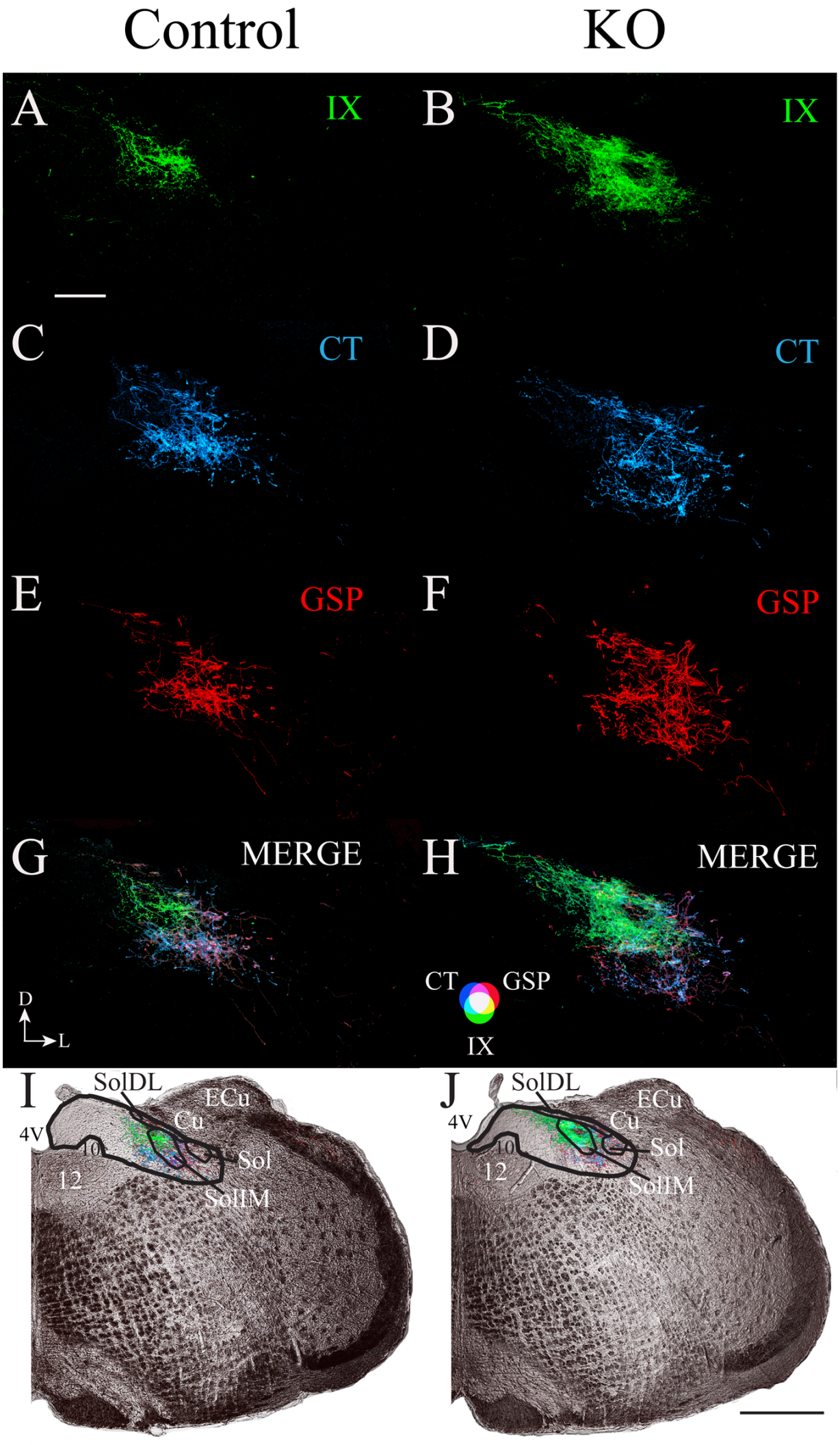
Control
KO
A
IX
B
IX
C
CT
D
CT
E
GSP
F
GSP
G
MERGE
H
MERGE
D
L
CT
GSP
IX
I
SolDL
ECu
Cu
4V
10
12
Sol
SolIM
J
SolDL
ECu
Cu
4V
10
12
Sol
SolIM